J. Appl. Comput. Mech., 5(2) (2019) 207-216
DOI: 10.22055/JACM.2018.26184.1310

ISSN: 2383-4536
jacm.scu.ac.ir

M&MoCS

Shahid Chamran University of Ahvaz

Journal of Applied and Computational Mechanics

Research Paper

# Effect of Thermal Conductivity and Emissivity of Solid Walls on Time-Dependent Turbulent Conjugate Convective-Radiative Heat Transfer

**Igor V. Miroshnichenko, Mikhail A. Sheremet**

Laboratory on Convective Heat and Mass Transfer, Tomsk State University, 634050, Tomsk, Russia

Received June 08 2018; Revised July 24 2018; Accepted for publication July 28 2018.
Corresponding author: Mikhail A. Sheremet, Michael-sher@yandex.ru


**Abstract.** In the present study, the conjugate turbulent free convection with the thermal surface radiation in a rectangular enclosure bounded by walls with different thermophysical characteristics in the presence of a local heater is numerically studied. The effects of surface emissivity and wall materials on the air flow and the heat transfer characteristics are the main focus of the present investigation. The conjugate convective heat transfer for the fluid (air), described in terms of linear momentum, continuity, and energy equations combined with k-ε turbulence model, is predicted by using the finite difference method. The results for the isotherms, streamlines, and average Nusselt numbers along the heat source are presented. The numerical experiments show that an increase in thermal conductivity of solid walls illustrates the enhancement of heat transfer. Eventually, the main result obtained in this work provides a good technical support for the development and research of energy-efficient building materials.

**Keywords**: Natural convection; Surface radiation; Turbulence; Heat source; Thermal conductivity; Finite difference method.

## 1. Introduction

The turbulent free convection in enclosures has received extensive research over the past two decades owing to its paramount importance and applications in the energy transfer in buildings. The distribution of temperature plays an important role in the heat exchange between the building and the environment, which affects the energy consumption of buildings. Therefore, it is necessary that houses are energy efficient; viz. the energy consumption for house heating should be kept to a minimum. Thermal conditions in rooms are significant topics of urban microclimate and have a great impact on the thermal comfort of building constructions.

It should be mentioned that numerous experimental studies of free convection as well as radiation in enclosures have been carried out [1–5]. Tian and Karayiannis [6] studied the turbulent free convection in a square cavity with dimensions of 0.75 m × 0.75 m × 1.5 m. The temperature distributions in the cavity, average, and local Nusselt numbers were obtained. It was established that their results are good experimental benchmark data which help to check the CFD code. The work of Awbi and Hatton [7] was devoted to study of free convection of heated room surfaces to determine convective heat transfer coefficients for calculating the air flow and the thermal conditions in a room. Therefore, they recommended that in the design calculations, the accurate values of convective heat transfer coefficients must be used. Moreover, the currently used values in most thermal building models must be revised. Obyn and van Moeseke [8] also investigated the effect of convective heat transfer coefficients on the assessment of energy consumption of buildings. The experimental study of the turbulent free convection in enclosure with a heat source was carried out by Zhang et al. [9] using PIV measurement technique and detailed information about the distribution of temperature and velocity was obtained.

Recent developments in processing power and algorithms make it possible to simulate real physical processes at levels of

Published online: January 19 2019

detail that were almost impossible just a few years ago. In this connection, the numerical simulation of free convection in enclosures has received considerable attention from many researchers [1, 10–13]. Wang et al. [14] studied free convection and surface radiation in a three-dimensional industrial building with a local heat source. The effects of Grashof number in a wide range between $10^7$ and $10^{11}$, and the surface emissivity in a range between 0.2 and 0.8 on the fluid flow and the heat transfer were extensively explored. The results indicated that an increase in Grashof number leads to growth of the average convective Nusselt number. Free convection in rectangular cavities with different aspect ratios was investigated by Manz [15]. The author compared the average Nusselt numbers as a function of *Ra* with five correlations from other experimental works. With the exception of one correlation, all Nusselt numbers deviates less than 20% from the correlations.

Kogawa et al. [16] studied the effect of radiation on the turbulent free convection in cubic enclosure with uniform heated and cooled walls. They showed that the influence of surface radiation on the total heat transfer was dominant, at the same time the effect of the gas radiation was small. Ben-Nakhi and Mahmoud [17] investigated the effects of Rayleigh number, cavity aspect ratio, and external wall construction materials on the conjugate turbulent free convection inside a rectangular enclosure under winter day boundary conditions. Their findings indicated that all these key parameters have significant effect on streamlines and isotherms in the enclosure, and the heat flux out of the room through the enclosure. The numerical simulation of turbulent free convection in 2D and 3D rectangular enclosures was carried out by Altac and Ugurlubilek [18]. There are six RANS turbulence models have been compared with published experimental both two- and three-dimensional numerical results. It is worth noting that the comparisons indicate a very good agreement between the available data and obtained numerical solutions of all RANS turbulence models for $Ra < 10^{11}$. To calculate the free convection heat transfer coefficients in enclosures new correlations were presented by Rincon-Casado et al. [19]. They showed that for low Rayleigh numbers ($Ra < 10^7$), the Nusselt number depends on the aspect ratio, while for high Rayleigh numbers ($Ra > 10^7$) this dependency is low. Ultimately, the results were implemented in the thermal simulation software for the building industry. Sharma et al. [20] investigated the turbulent free convection in an enclosure with the local heat source. The results were reported in the form of streamlines, isotherms, and average Nusselt numbers at the heat source surface. It was obtained that the flow intensity increases linearly with a growth of the heated width. A numerical study of turbulent forced convection in an enclosure with ventilation ports was carried out by Sourtiji et al. [21]. They found out that the total heat transfer rate and the pressure drop in an enclosure significantly depend on the Reynolds number (*Re*) and the location of the outlet port. A detailed review of both experimental and numerical research of the turbulent free convection in rectangular enclosures can be found in [1].

Enclosures with triangular cross-section were also investigated in many studies [22–24] to model thermodynamic conditions inside attic spaces. A detailed review of these research can be found in [25]. It was found from the review that most works are performed in the laminar regimes. At the same time, in practice, the air flow inside the attic is turbulent with the higher Rayleigh numbers. Therefore, further research should be performed for turbulent modes.

Engineering and industrial applications of free convection require solving combined problems of the fluid mechanics and the heat transfer that depend on several parameters among which radiative properties of medium and solid walls, aspect ratio of the enclosure, values of the Rayleigh number and so on. The position of local heater also plays an important role in determining the nature of heat transfer. Therefore, a specific analysis is needed for each application.

The objective of the present study is to investigate the turbulent modes of the conjugate free convection combined with the thermal surface radiation in an enclosure bounded by walls from various building materials with a local heater. The above-mentioned literature indicates that this problem has not been studied in detail. Therefore, it is still necessary to quantify well the effects of surface radiation and thermal conductivity ratio on the heat transfer and fluid flow in cavities similar to the many real houses or other industrial applications.

## 2. Definition of physical model

The geometry of the problem for the numerical study is depicted in Fig. 1. This is an enclosure bounded by solid walls of finite thickness $l$ and $2l$, and different values of conductivity $\lambda_1$ and surface emissivity $\tilde{\varepsilon}_1$. In this model, the heat source of constant temperature $T_{hs}$ and length of $0.4L$ is located on the internal surface of the left wall. The external surfaces of the right, top, and bottom walls are considered to be adiabatic, whereas the convective heat exchange with an environment is modeled on border $x = 0$. The upper part of the left wall is a glass conductive wall of thickness $l$, conductivity $\lambda_2$, and surface emissivity $\tilde{\varepsilon}_2$. The working fluid in the enclosure is the air ($Pr = 0.71$). It is assumed that all air properties are constant, with the exception of the density, which depends on the temperature difference under the Boussinesq approximation. The internal surfaces of the heat source and all walls are considered to be both gray diffusive emitters and reflectors of radiation. The ambient temperature $T^e$ is assumed to be both constant and less than an initial temperature in the considered area. For the radiative effect, there are two assumptions: firstly, the air flow inside the enclosure is considered radiatively non-participating, and secondly, the glass wall is not transparent to radiation. It should be mentioned that the air flow in building is often turbulent. Therefore, to predict the turbulent fluxes and stresses, the standard $k$–ε model is used due to its useful application in similar problems [26–29].

## 3. Governing equations and solution method

A two-dimensional conjugate turbulent free convection with the thermal surface radiation in the enclosure with a heat source is considered in the present study. For the unsteady turbulent fluid flow, taking the size of the enclosure ($L$), the mean velocity $\left(V_0 = \sqrt{g\beta\left(T_{hs} - T^e\right)L}\right)$, and the time period $\left(t_0 = \sqrt{g\beta\left(T_{hs} - T^e\right)/L}\right)$ as characteristics of length, velocity, and

time, respectively, the following non-dimensional variables are expressed as follows:

$$X = x/L,\ Y = y/L,\ \tau = t\sqrt{g\beta\left(T_{hs}-T^{e}\right)/L},\ U = u\Big/\sqrt{g\beta\left(T_{hs}-T^{e}\right)L},$$
$$V = v\Big/\sqrt{g\beta\left(T_{hs}-T^{e}\right)L},\ \Theta = \left(T-T^{e}\right)\Big/\left(T_{hs}-T^{e}\right),\Psi = \psi\Big/\sqrt{g\beta\left(T_{hs}-T^{e}\right)L^{3}}, \tag{1}$$
$$\Omega = \omega\sqrt{L\Big/g\beta\left(T_{hs}-T^{e}\right)},\ K = k\Big/\left(g\beta\left(T_{hs}-T^{e}\right)L\right),\ E = \varepsilon\Big/\sqrt{g^{3}\beta^{3}\left(T_{hs}-T^{e}\right)^{3}L}.$$

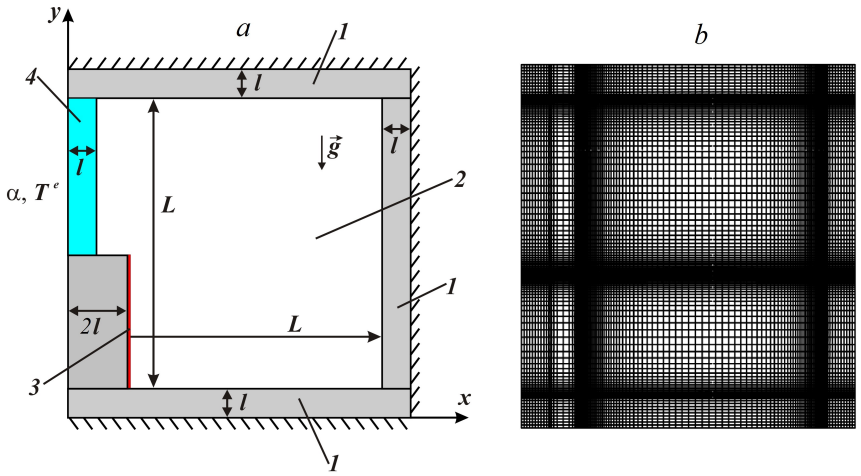


**Fig. 1.** The domain of interest (*a*): *1* – solid walls, *2* – air cavity, *3* – heat source of constant temperature, *4* – glass wall; computational domain with a non-uniform grid (*b*)

To solve the problem under consideration, it is better to use many nodes near the internal surface of both the walls and the heat source. Therefore, the concrete coordinate transformation is applied for the computational domain [27–29]:

$$\xi = a + \frac{b-a}{2}\left\{1+\mathrm{tg}\left[\frac{\pi\kappa}{b-a}\left(X-\frac{a+b}{2}\right)\right]\Big/\mathrm{tg}\left[\frac{\pi}{2}\kappa\right]\right\},$$
$$\eta = a + \frac{b-a}{2}\left\{1+\mathrm{tg}\left[\frac{\pi\kappa}{b-a}\left(Y-\frac{a+b}{2}\right)\right]\Big/\mathrm{tg}\left[\frac{\pi}{2}\kappa\right]\right\}. \tag{2}$$

It should be noted that in case $\kappa\to 1$, the substantially non-uniform mesh with a lot of points close to the walls and few points in the central part of the domain is provided, and in case $\kappa\to 0$, a uniform mesh in physical domain is prepared. The governing equations in the temperature-stream function-vorticity formulation, taking into account specific transformation (2), are as follows:

– inside the air cavity (*2* in Fig. 1)

$$\frac{d^{2}\xi}{dX^{2}}\frac{\partial\Psi}{\partial\xi}+\left(\frac{d\xi}{dX}\right)^{2}\frac{\partial^{2}\Psi}{\partial\xi^{2}}+\frac{d^{2}\eta}{dY^{2}}\frac{\partial\Psi}{\partial\eta}+\left(\frac{d\eta}{dY}\right)^{2}\frac{\partial^{2}\Psi}{\partial\eta^{2}}=-\Omega \tag{3}$$

$$\frac{\partial\Theta}{\partial\tau}+U\frac{d\xi}{dX}\frac{\partial\Theta}{\partial\xi}+V\frac{d\eta}{dY}\frac{\partial\Theta}{\partial\eta}=\frac{d\xi}{dX}\frac{\partial}{\partial\xi}\left[\left(\frac{1}{\sqrt{Ra\cdot Pr}}+\frac{\nu_{t}}{Pr_{t}}\right)\frac{d\xi}{dX}\frac{\partial\Theta}{\partial\xi}\right]+\frac{d\eta}{dY}\frac{\partial}{\partial\eta}\left[\left(\frac{1}{\sqrt{Ra\cdot Pr}}+\frac{\nu_{t}}{Pr_{t}}\right)\frac{d\eta}{dY}\frac{\partial\Theta}{\partial\eta}\right] \tag{4}$$

$$\frac{\partial\Omega}{\partial\tau}+\left(U-\frac{d\xi}{dX}\frac{\partial\nu_{t}}{\partial\xi}\right)\frac{d\xi}{dX}\frac{\partial\Omega}{\partial\xi}+\left(V-\frac{d\eta}{dY}\frac{\partial\nu_{t}}{\partial\eta}\right)\frac{d\eta}{dY}\frac{\partial\Omega}{\partial\eta}=\frac{d\xi}{dX}\frac{\partial}{\partial\xi}\left[\left(\sqrt{\frac{Pr}{Ra}}+\nu_{t}\right)\frac{d\xi}{dX}\frac{\partial\Omega}{\partial\xi}\right]+\frac{d\eta}{dY}\frac{\partial}{\partial\eta}\left[\left(\sqrt{\frac{Pr}{Ra}}+\nu_{t}\right)\frac{d\eta}{dY}\frac{\partial\Omega}{\partial\eta}\right]$$
$$+\left(\frac{d^{2}\xi}{dX^{2}}\frac{\partial\nu_{t}}{\partial\xi}+\left(\frac{d\xi}{dX}\right)^{2}\frac{\partial^{2}\nu_{t}}{\partial\xi^{2}}-\frac{d^{2}\eta}{dY^{2}}\frac{\partial\nu_{t}}{\partial\eta}-\left(\frac{d\eta}{dY}\right)^{2}\frac{\partial^{2}\nu_{t}}{\partial\eta^{2}}\right)\times\left(\Omega+2\frac{d\eta}{dY}\frac{\partial U}{\partial\eta}\right)+4\frac{d\xi}{dX}\left(\frac{d\eta}{dY}\right)^{2}\frac{\partial^{2}\nu_{t}}{\partial\xi\partial\eta}\frac{\partial V}{\partial\eta}+\frac{d\xi}{dX}\frac{\partial\Theta}{\partial\xi} \tag{5}$$

$$\frac{\partial K}{\partial\tau}+U\frac{d\xi}{dX}\frac{\partial K}{\partial\xi}+V\frac{d\eta}{dY}\frac{\partial K}{\partial\eta}=\frac{d\xi}{dX}\frac{\partial}{\partial\xi}\left[\left(\sqrt{\frac{Pr}{Ra}}+\frac{\nu_{t}}{\sigma_{k}}\right)\frac{d\xi}{dX}\frac{\partial K}{\partial\xi}\right]+\frac{d\eta}{dY}\frac{\partial}{\partial\eta}\left[\left(\sqrt{\frac{Pr}{Ra}}+\frac{\nu_{t}}{\sigma_{k}}\right)\frac{d\eta}{dY}\frac{\partial K}{\partial\eta}\right]+P_{k}+G_{k}-E \tag{6}$$

$$\frac{\partial E}{\partial\tau}+U\frac{d\xi}{dX}\frac{\partial E}{\partial\xi}+V\frac{d\eta}{dY}\frac{\partial E}{\partial\eta}=\frac{d\xi}{dX}\frac{\partial}{\partial\xi}\left[\left(\sqrt{\frac{Pr}{Ra}}+\frac{\nu_{t}}{\sigma_{\varepsilon}}\right)\frac{d\xi}{dX}\frac{\partial E}{\partial\xi}\right]+\frac{d\eta}{dY}\frac{\partial}{\partial\eta}\left[\left(\sqrt{\frac{Pr}{Ra}}+\frac{\nu_{t}}{\sigma_{\varepsilon}}\right)\frac{d\eta}{dY}\frac{\partial E}{\partial\eta}\right]+c_{1\varepsilon}\left(P_{k}+c_{3\varepsilon}G_{k}\right)\frac{E}{K}-c_{2\varepsilon}\frac{E^{2}}{K} \tag{7}$$

– inside the solid walls (*1* in Fig. 1)

$$\frac{\partial\Theta}{\partial\tau}=\frac{\alpha_{1,2}}{\sqrt{Ra\cdot Pr}}\left(\frac{d^2\xi}{dX^2}\frac{\partial\Theta}{\partial\xi}+\left(\frac{d\xi}{dX}\right)^2\frac{\partial^2\Theta}{\partial\xi^2}+\frac{d^2\eta}{dY^2}\frac{\partial\Theta}{\partial\eta}+\left(\frac{d\eta}{dY}\right)^2\frac{\partial^2\Theta}{\partial\eta^2}\right). \tag{8}$$

here

$$P_k=\nu_t\left[2\left(\frac{d\xi}{dX}\frac{\partial U}{\partial\xi}\right)^2+2\left(\frac{d\eta}{dY}\frac{\partial V}{\partial\eta}\right)^2+\left(\frac{d\eta}{dY}\frac{\partial U}{\partial\eta}+\frac{d\xi}{dX}\frac{\partial V}{\partial\xi}\right)^2\right],$$
$$G_k=-\frac{\nu_t}{\mathrm{Pr}_t}\frac{d\eta}{dY}\frac{\partial\Theta}{\partial\eta},\quad \nu_t=c_\mu\frac{K^2}{E},\quad y^+=\frac{yu^*}{\nu}=\sqrt[4]{\frac{\mathrm{Ra}}{\mathrm{Pr}}}Y\sqrt{\frac{\partial U}{\partial Y}}. \tag{9}$$

The coefficients $c_\mu$, $c_{1s}$, $c_{2s}$, $c_{3s}$, $\sigma_k$, $\sigma_\varepsilon$, and $Pr_t$ are constants which have the following empirical values [26], $c_\mu = 0.09$, $c_{1s} = 1.44$, $c_{2s} = 1.92$, $c_{3s} = 0.8$, $\sigma_k = 1.0$, $\sigma_\varepsilon = 1.3$, $Pr_t = 1.0$. The governing Eqs. (3) to (8) are complemented by both boundary and initial conditions.

Initial conditions:

$$\Psi(\xi,\eta,0)=\Omega(\xi,\eta,0)=K(\xi,\eta,0)=E(\xi,\eta,0)=0,\ \Theta(\xi,\eta,0)=0.5 \tag{10}$$

Boundary conditions:

- at the boundaries $X = 0$: $(\partial\xi/\partial X)\times(\partial\Theta/\partial\xi)=Bi\cdot\Theta$ (the convective heat exchange with an environment is modeled on the external surface of the left wall);
- at the boundary $X = 1+2l/L$: $\partial\Theta/\partial\xi=0$ (the external surface of the right wall is adiabatic);
- at the boundary $Y = 0$: $(\partial\Theta/\partial\eta)=0$ (the external surface of the bottom wall is adiabatic);
- at the boundary $Y = 1+2l/L$: $(\partial\Theta/\partial\eta)=0$ (the external surface of the top wall is adiabatic);
- at the heat source surface: $\Theta = 1$;
- at the internal borders of the solid material and air, parallel to the axis *OX*:

$$\Psi=0,\ K=0,\ \frac{\partial\Psi}{\partial\eta}=0,\ \frac{\partial E}{\partial\eta}=0,\ \Theta_s=\Theta_f,\ \lambda_{sf}\frac{\partial\eta}{\partial Y}\frac{\partial\Theta_s}{\partial\eta}=\frac{\partial\eta}{\partial Y}\frac{\partial\Theta_f}{\partial\eta}-N_{rad}Q_{rad}; \tag{11}$$

- at the internal borders of the solid material and air, parallel to the axis *OY*:

$$\Psi=0,\ K=0,\ \frac{\partial\Psi}{\partial\xi}=0,\ \frac{\partial E}{\partial\xi}=0,\ \Theta_s=\Theta_f,\ \lambda_{sf}\frac{\partial\xi}{\partial X}\frac{\partial\Theta_s}{\partial\xi}=\frac{\partial\xi}{\partial X}\frac{\partial\Theta_f}{\partial\xi}-N_{rad}Q_{rad}. \tag{12}$$

The heat transfer rate at the heat source surface is presented by means of average radiative and convective Nusselt numbers, which are obtained from:

$$Nu_{conv}=\int_{l/L}^{l/L+0.4}\left|\frac{\partial\xi}{\partial X}\frac{\partial\Theta}{\partial\xi}\right|_{\xi=\xi_{hs}}d\eta,\quad Nu_{rad}=N_{rad}\int_{l/L}^{l/L+0.4}Q_{rad}\big|_{\xi=\xi_{hs}}d\eta \tag{13}$$

To determine the radiative heat flux, the net radiation method [27–30] is used. Here, the internal surfaces of solid walls are supposed to be gray and diffuse. It should be mentioned that the radiative heat flux of one radiation element is calculated by the emitted radiative energy and absorbed energy that comes from all other radiation elements. The dimensionless net-radiative heat flux $Q_{rad}$ is determined as follows [27–30]:

$$Q_{rad,k}=R_k-\sum_{i=1}^{N}F_{k-i}R_i$$
$$R_k=(1-\tilde{\varepsilon}_k)\sum_{i=1}^{N}F_{k-i}R_i+\tilde{\varepsilon}_k(1-\zeta)^4\left(\Theta_k+0.5\frac{1+\zeta}{1-\zeta}\right)^4. \tag{14}$$

where $R_k$ is a radiosity of the *k*th element of an enclosure, $F_{k-i}$ is a view factor from *k*th element to the *i*th element of an enclosure, and $\zeta$ is a temperature parameter. The view factor $F_{k-i}$ is the fraction of energy exiting from surface "*k*" (by reflection or emission) that directly falls on surface "*i*" (to be reflected, absorbed, or transmitted). It is worth noting that the view factors depend only on geometry. The crossed string method [27–30] is applied to determine $F_{k-i}$. This method is illustrated in Fig. 2. The view factors $F_{k-j}$ between the surface elements $A_k$ and $A_j$ is calculated by the following formula:

$$F_{k-j}A_k=\frac{AD+BC-AC-BD}{2} \tag{15}$$

The partial differential Eqs. (3) to (8) are solved using the finite-difference method. In particular, the Poisson equation for the stream function $\Psi$ in Eq. (3) is discretized using the central differences for the second derivatives. To solve the resulting linear discretized equation, the successive over relaxation method is applied. The remaining parabolic Eqs. (4) to (8) are solved using Samarskii's locally one-dimensional scheme [31]. To approximate the diffusion and convective terms, the central differences and the Samarskii's monotone scheme are used, respectively. To solve the resulting linear discretized equations, Thomas algorithm is used. The optimum value of the relaxation parameter is chosen on the basis of computing experiments.

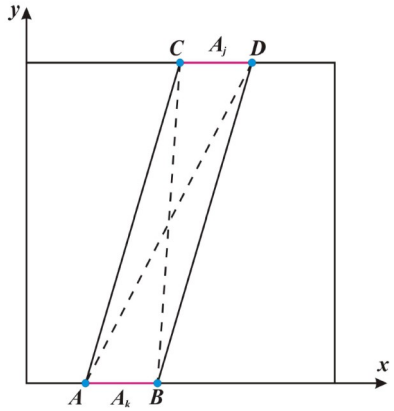


**Fig. 2.** Illustration of Hottel crossed string method

To test the grid independence of the numerical scheme, three different grid sizes of 90×90, 120×120, and 180×180 points are used. The average radiative and convective Nusselt numbers at the heat source surface predicted by these mesh structures are compared in Table 1. Based on these numerical experiments, the difference in the average convective Nusselt number between the grid pattern of 90×90 and that of 180×180 is 3.66%, whereas between the 120×120 grid and 180×180 grid is only 0.52%. The results showed that the grid of 120×120 points provided a satisfactory compromise as the basic grid between the computational efforts required to model the complex heat transfer without the use of extremely small time steps and accuracy. Therefore, non-uniform grid of 120×120 points with the time step $\tau = 10^{-3}$ is selected.

**Table 1.** Results of the grid independence study for $Ra = 3 \cdot 10^9$, $\lambda_1 = 0.15$ and $\lambda_2 = 1.15$

| Grid size | $Nu_{conv}$ | % Change | $Nu_{rad}$ | % Change |
|---|---|---|---|---|
| 90×90 | 75.63 | – | 104.58 | – |
| 120×120 | 73.24 | 3.16 | 104.16 | 0.40 |
| 180×180 | 72.86 | 0.52 | 104.03 | 0.12 |

For validation of this mathematical model and computational technique, the following tests are performed [27–29, 32]. The first test is performed to make a comparison with the experimental data of Ampofo and Karayiannis [33] for the turbulent free convection in a square enclosure without the heat source. It is worth noting that the temperature and velocity profiles are close to the experimental data (Fig. 3). Moreover, a comparison of the average Nusselt number with the published results for the case of turbulent free convection without radiation is presented in Table 2. The enclosures of these validation cases are filled with air. The air inside the cavity is considered as the homogeneous isotropic medium that behaves as a Newtonian and incompressible fluid. The left vertical wall is kept isothermal with high temperature $T_h$, and the right vertical wall is kept isothermal with low temperature $T_c$. The horizontal walls are assumed to be perfectly insulated.

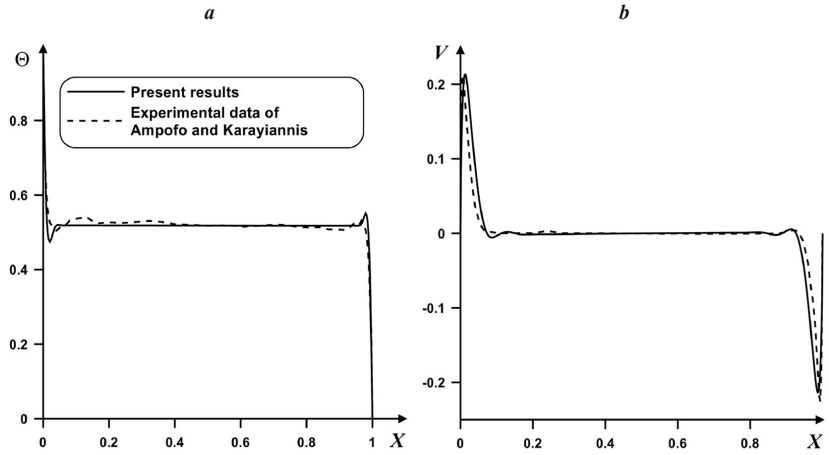


**Fig. 3.** The temperature profiles (*a*) and vertical velocity profiles (*b*) at $Ra = 1.58 \cdot 10^9$ in comparison with the experimental data of Ampofo and Karayiannis [33]

**Table 2.** Comparison of average Nusselt number with published data for turbulent free convection in a differentially heated cavity

| *Ra* | [34] | [35] | [36] | Present data |
|---|---|---|---|---|
| $10^7$ | 16.79 | 16.523 | 16.39 | 17.13 |
| $10^8$ | 30.506 | 30.225 | 29.97 | 33.06 |
| $10^9$ | 57.35 | – | – | 60.54 |

Taking into account the performed verification, the developed mathematical model and the computational technique can be used for the numerical simulation of turbulent convective-radiative heat transfer within a cavity with a local heater.

## 4. Results and discussion

Numerical results in terms of the streamline and temperature contours for various values of the surface emissivity and the thermal conductivity are presented below. The fluid to be used is the air with Prandtl number $Pr = 0.71$. The effects of material type used for construction of the solid wall on the streamlines and temperature contours are analyzed. The results for both the average radiative $Nu_{rad}$ and the convective $Nu_{conv}$ Nusselt numbers for various conditions are discussed. The different surface emissivity $\tilde{\varepsilon}_1$ values (0, 0.3, 0.6 and 0.8) of the internal surfaces of solid walls are used to investigate the influence of radiation on the thermal behavior, while $\tilde{\varepsilon}_2 = 0.9$.

The effect of dimensionless time on isotherms and streamlines at $Ra = 3 \cdot 10^9$, $\tilde{\varepsilon}_1 = 0.6$, $\lambda_1 = 0.55$, $\lambda_2 = 1.15$ is shown in Fig. 4. It can be seen that two convective cells (counterclockwise in the left half and clockwise in the right half) are formed in the cavity due to the heating from the heat source and the cooling from the outside. At the initial period of time ( $\tau < 2000$ ), the dimension of one convective cell strongly exceeds the dimension of the other one. Further increase in the dimensionless time ($\tau > 2000$) result in an increase in the size of counterclockwise cells due to strong cooling from the ambient. The distributions of temperature reflect a formation of the ascending warm flow near the local heater. This leads to a creation of the thermal plume which extends closer to the right and top walls. It should be noted that the further increase in the dimensionless time up to 10000 (Fig. 4*c*) result in a formation of the stationary heat transfer mode (the thermal plume is located horizontally).

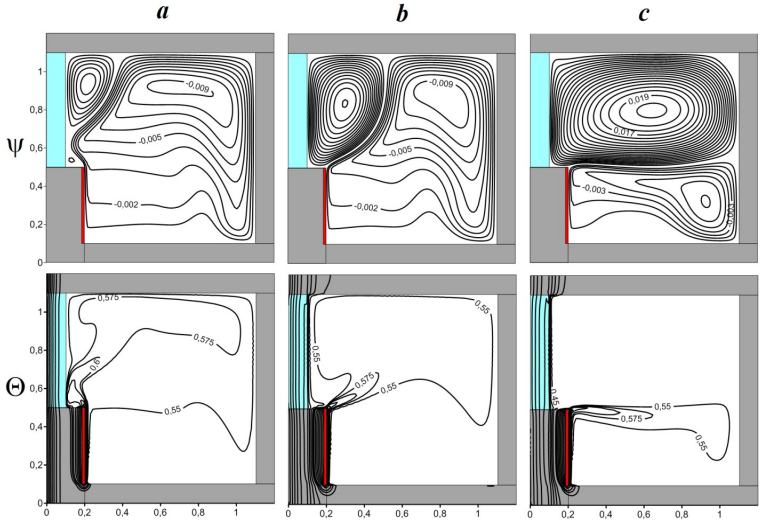


**Fig. 4.** Streamlines Ψ and isotherms Θ at $Ra = 3 \cdot 10^9$, $\tilde{\varepsilon}_1 = 0.6$, $\lambda_1 = 0.55$, $\lambda_2 = 1.15$: $\tau = 2000$ – *a*, $\tau = 6000$ – *b*, $\tau = 10000$ – *c*

More detailed effect of the dimensionless time on the temperature distributions at middle cross-section $X = 0.6$ is presented in Fig. 5. It is clear that the essential cooling of the top part of the enclosure occurs at $\tau = 10000$ due to a decrease in the temperature of the glass wall owing to the low temperature penetration from external environment.

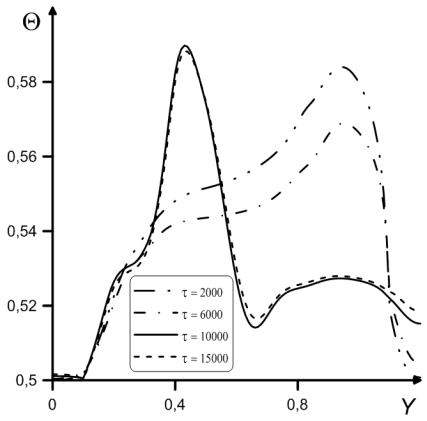


**Fig. 5.** Temperature profiles at $X = 0.6$ for $Ra = 3 \cdot 10^9$, $\tilde{\varepsilon}_1 = 0.6$, $\lambda_1 = 0.55$, $\lambda_2 = 1.15$, and different values of dimensionless time

The distributions of isotherms Θ, streamlines Ψ, and isolines of turbulent viscosity $\nu_t$ at different values of thermal conductivity of solid walls are shown in Fig. 6. Regardless of the thermal conductivity values, the cooling effect of the cavity glass wall creates a downward flow because of buoyancy effects, thus creating a counterclockwise-rotating vortex in the left upper corner of the enclosure. The power of this vortex increases progressively with $\lambda_1$. Moreover, the growth of an air circulation rate $\left|\Psi\right|_{\max}^{\lambda_1=0.15} = 0.003 < \left|\Psi\right|_{\max}^{\lambda_1=0.55} = 0.010 < \left|\Psi\right|_{\max}^{\lambda_1=1.5} = 0.021$ is observed at the changing of solid walls thermal

conductivity from 0.15 to 1.5. Figure 6 indicates that an increase in $\lambda_1$ results in more essential cooling of the enclosure top part. It is worth noting that for high values of the thermal conductivity of solid walls one can find more intensive penetration of the low temperature wave from the outside.

When the flow is turbulent, the diffusion mechanism is realized not only by molecular motions, and also strongly enhanced by the motions of the vortices. The turbulent viscosity $\nu_t$ is added to the molecular viscosity in momentum and energy equations and intensifies the diffusion mechanism in these equations. It can be seen that at $\lambda_1 = 0.15$, the region of high turbulent viscosity is located both in the left upper corner and near the right wall. A further growth of thermal conductivity of solid walls up to 1.5 result in the fact that the high values of $\nu_t$ are in the middle part of the enclosure.

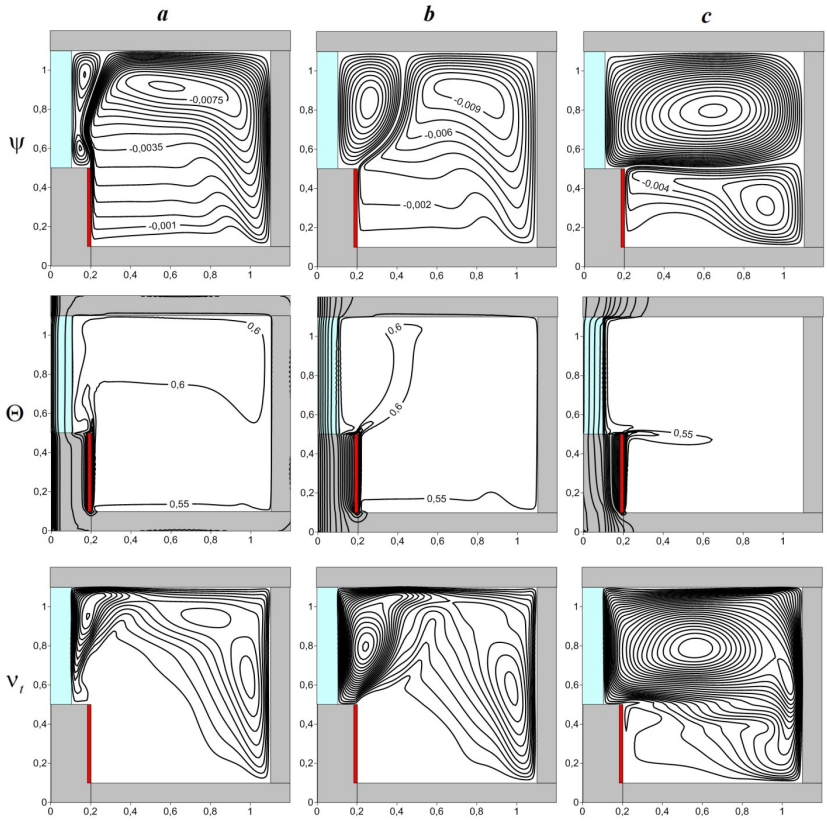


**Fig. 6.** Streamlines Ψ, isotherms Θ, and turbulent viscosity $\nu_t$ at $\tau = 4000$, $\tilde{\varepsilon}_1 = 0.6$ , $Ra = 3 \cdot 10^9$, $\lambda_2 = 1.15$: $\lambda_1 = 0.15$ – *a*, $\lambda_1 = 0.55$ – *b*, $\lambda_1 = 1.5$ – *c*

The variation of the average radiative Nusselt number, convective Nusselt number, and total Nusselt number as a function of the thermal conductivity for Rayleigh number $Ra = 3 \cdot 10^9$ at $\tau = 10000$ is presented in Table 3. An increase in $\lambda_1$ results in a growth of both the average radiative and convective Nusselt numbers. This is due to a decrease in the thermal resistance of the solid walls of the enclosure, leading to a reduction of temperature at the surface of the walls. Furthermore, an increment in the temperature difference near the walls occurs, which leads to an intensification of both free convection and thermal radiation heat transfer. In particular, at $\tau = 10000$, the average radiative Nusselt number increases up to 44% by changing of the thermal conductivity of solid walls from 0.15 to 1.5. This trend is also consistent with the previously presented results [28, 37].

**Table 3.** The average Nusselt numbers as a function of thermal conductivity

| Fixed parameter | Thermal conductivity of solid walls | Radiative Nusselt number, $Nu_{rad}$ | Convective Nusselt number, $Nu_{conv}$ | Total Nusselt number, $Nu_{total}$ | % Increase in heat transfer |
|---|---|---|---|---|---|
| $Ra = 3 \cdot 10^9$ | $\lambda_1 = 0.15$ | 104.16 | 73.24 | 177.4 | 0 |
| $\lambda_2 = 1.15$ | $\lambda_1 = 0.55$ | 123.95 | 72.16 | 196.11 | 10 |
| $\tilde{\varepsilon}_1 = 0.6$ $\tau = 10000$ | $\lambda_1 = 1.5$ | 149.94 | 94.67 | 244.61 | 37 |

The surface radiation plays an essential role in the heat transfer process in closed enclosures. Therefore, the effect of surface radiation on heat and fluid flow is an important topic in numerous experimental and numerical studies [1, 9, 10, 27, 28]. Figure 7 shows contour plots for the isotherms, streamlines, and turbulent viscosity isolines for $Ra = 3 \cdot 10^9$ and for values of surface emissivity $\tilde{\varepsilon}_1$ from 0 to 0.8. It is worth noting that the radiation effect is negligible when the surface emissivity is equal to zero. As already mentioned above, two convective cells (clockwise and counterclockwise) are formed in the enclosure. An increase in $\tilde{\varepsilon}_1$ results in both the augmentation of the one cell (counterclockwise) and the detriment of another one (clockwise). The heat transfer by free convection and radiation from the heat source surface affects the temperature field differently. The heat transfer by radiation affects the solid walls temperature first, and causes heat exchange between medium

(air) and solid walls in the form of convection in the second case. At the same time, the heat transfer by convection is based on the fluid (air) density difference due to changes of fluid (air) temperature. Therefore, an increase in the surface emissivity $\tilde{\varepsilon}_1$ leads to more intensive heating of the analyzed enclosure that is caused by the physical features of the surface radiation described above. It is evident that average radiative Nusselt number increases with the growth of surface emissivity of solid walls. This dependence can be seen in the Fig. 8. At $\tau = 10000$, the average radiative Nusselt number increases up to 2.33 times by changing of $\tilde{\varepsilon}_1$ from 0.3 to 0.8.

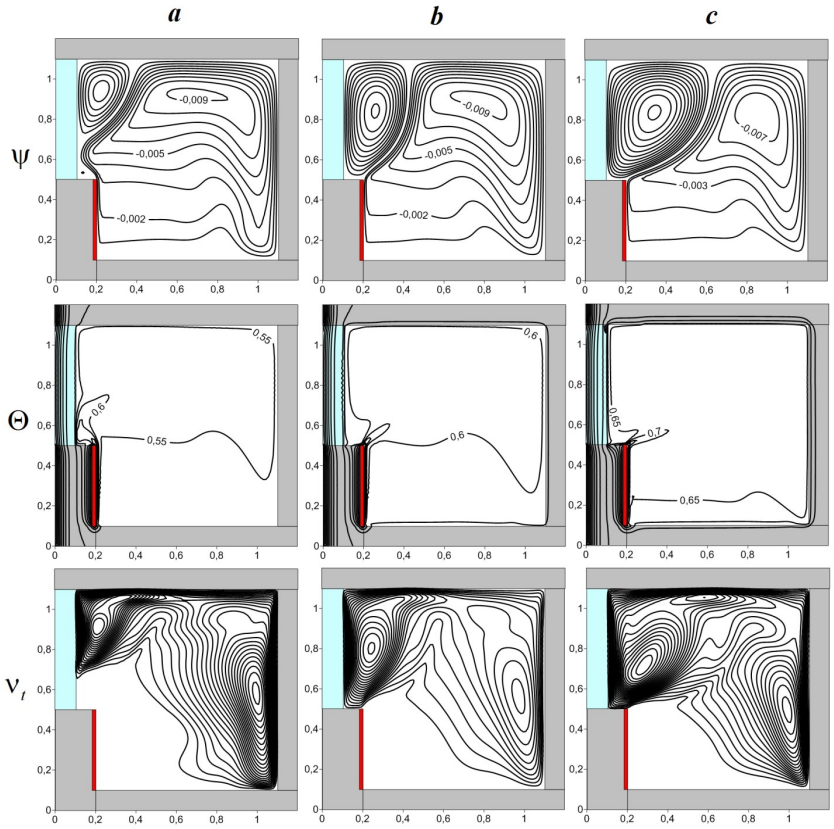


**Fig. 7.** Streamlines Ψ, isotherms Θ, and turbulent viscosity $\nu_t$ at $\tau = 10000$, $Ra = 3 \cdot 10^9$, $\lambda_1 = 0.15$, $\lambda_2 = 1.15$: $\tilde{\varepsilon}_1 = 0.0$ – *a*, $\tilde{\varepsilon}_1 = 0.3$ – *b*, $\tilde{\varepsilon}_1 = 0.8$ – *c*

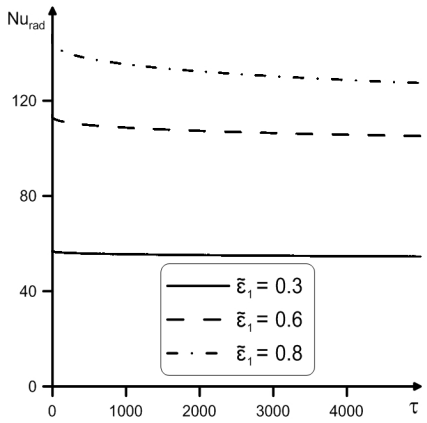


**Fig. 8.** Variation of the average radiative Nusselt number at the heater surface vs. the dimensionless time and surface radiation at $\tau = 5000$, $Ra = 3 \cdot 10^9$, $\lambda_1 = 0.15$, $\lambda_2 = 1.15$

## 5. Conclusions

In order to evaluate the effects of thermal conductivity and surface emissivity of bounded solid walls on the turbulent free convection and the thermal radiation in an enclosure, the numerical simulation using the RANS approach was carried out in this study. The stream function and vorticity variables with very efficient algebraic coordinate transformation were employed in order to create a non-uniform mesh inside the physical domain and the uniform mesh within the computational domain. Such method allows reducing the computational time substantially in comparison with using of the primitive variables. The numerical model was validated against benchmark experimental results. Contour plots for the streamlines, isotherms, and

turbulent viscosity isolines for several parametric conditions were presented and discussed. The total heat transfer, which includes the convective and radiative heat transfer rates, were investigated. Some important results of this study can be described as follows:

- The numerical experiments show that the effect of surface radiation enhances the flow instability inside the enclosure. At $\tau = 5000$, the average radiative Nusselt number increases up to 92% by changing of $\tilde{\varepsilon}_1$ from 0.3 to 0.6.
- Neglecting the surface radiation when trying to simulate airflow and thermal dynamics in the room does not provide an accurate description of the actual behavior of the flow or the level of air temperature in buildings.
- The growth of an air circulation rate is observed by changing the thermal conductivity of solid walls. The average convective Nusselt number increases up to 23% by changing the thermal conductivity of solid walls from 0.55 to 1.5.
- This study can be useful for practical applications. The parameters $\tilde{\varepsilon}_1$ and $\lambda_1$ are reasonable from a physical point of view. In particular, a red brick has $\tilde{\varepsilon}_1 \approx 0.55$ and $\lambda_1 \approx 0.9$.

The results clearly show an essential effect of surface radiation on the fluid flow and the heat transfer. This numerical technique would benefit engineers and scientists to become familiar with the analysis of turbulent convective-radiative heat transfer and can be widely used in engineering problems, such as the simulation of air flow in both heat-generating elements in the power engineering and the building insulation system.

## Acknowledgments

This work was supported by the Russian Science Foundation (Project No. 17-79-20141).

## Conflict of Interest

The authors declare no conflict of interest.

## References

[1] I.V. Miroshnichenko, M.A. Sheremet, Turbulent natural convection heat transfer in rectangular enclosures using experimental and numerical approaches: A review, *Renewable and Sustainable Energy Reviews* 82 (2018) 40–59.
[2] A.J.N. Khalifa, W.K. Sahib, Turbulent buoyancy driven convection in partially divided enclosures, *Energy Conversion and Management* 43 (2002) 2115–2121.
[3] N. Dimassi, L. Dehmani, Experimental heat flux analysis of a solar wall design in Tunisia, *Journal of Building Engineering* 8 (2016) 70–80.
[4] F. Ampofo, Turbulent natural convection in an air filled partitioned square cavity, *International Journal of Heat and Fluid Flow* 25 (2004) 103–114.
[5] G. Yang , Y. Huang, J. Wu, L. Zhang, G. Chen, R. Lv, A. Cai, Experimental study and numerical models assessment of turbulent mixed convection heat transfer in a vertical open cavity, *Building and Environment* 115 (2017) 91-103.
[6] Y.S. Tian, T.G. Karayiannis, Low turbulence natural convection in an air filled square cavity Part I: the thermal and fluid flow fields, *International Journal of Heat and Mass Transfer* 43 (2000) 849–866.
[7] H.B. Awbi, A. Hatton, Natural convection from heated room surfaces, *Energy and Buildings* 30 (1999) 233–244.
[8] S. Obyn, G. van Moeseke, Variability and impact of internal surfaces convective heat transfer coefficients in the thermal evaluation of office buildings, *Applied Thermal Engineering* 87 (2015) 258-272.
[9] X. Zhang, G. Su, J. Yu, Z. Yao, F. He, PIV measurement and simulation of turbulent thermal free convection over a small heat source in a large enclosed cavity, *Building and Environment* 90 (2015) 105–113.
[10] T. Wu, C. Lei, On numerical modeling of conjugate turbulent natural convection and radiation in a differentially heated cavity, *International Journal of Heat and Mass Transfer* 91 (2015) 454–466.
[11] A. Alberto, N.M.M. Ramos, R.M.S.F. Almeida, Parametric study of double-skin facades performance in mild climate countries, *Journal of Building Engineering* 12 (2017) 87–98.
[12] M.A.R. Sharif, W. Liu, Numerical study of turbulent natural convection in a side-heated square cavity at various angles of inclination, *Numerical Heat Transfer, Part A* 43 (2003) 693–716.
[13] S. Hawendi, S. Gao, Impact of an external boundary wall on indoor flow field and natural cross-ventilation in an isolated family house using numerical simulations, *Journal of Building Engineering* 10 (2017) 109–123.
[14] Y. Wang, X. Meng, X. Yang, J. Liu, Influence of convection and radiation on the thermal environment in an industrial building with buoyancy-driven natural ventilation, *Energy and Buildings* 75 (2014) 394–401.
[15] H. Manz, Numerical simulation of heat transfer by natural convection in cavities of facade elements, *Energy and Buildings* 35 (2003) 305–311.
[16] T. Kogawa, J. Okajima, A. Sakurai, A. Komiya, S. Maruyama, Influence of radiation effect on turbulent natural convection in cubic cavity at normal temperature atmospheric gas, *International Journal of Heat and Mass Transfer* 104 (2017) 456–466.
[17] A. Ben-Nakhi, M.A. Mahmoud, Conjugate turbulent natural convection in the roof enclosure of a heavy construction building during winter, *Applied Thermal Engineering* 28 (2008) 1522–1535.
[18] Z. Altac, N. Ugurlubilek, Assessment of turbulence models in natural convection from two- and three-dimensional rectangular enclosures, *International Journal of Thermal Sciences* 107 (2016) 237–246.

[19] A. Rincón-Casado, F.J. Sánchez de la Flor, E. Chacón Vera, J. Sánchez Ramos, New natural convection heat transfer correlations in enclosures for building performance simulation, *Engineering Applications of Computational Fluid Mechanics* 11 (2017) 240-356.
[20] A.K. Sharma, K. Velusamy, C. Balaji, Turbulent natural convection in an enclosure with localized heating from below, *International Journal of Thermal Sciences* 46 (2007) 1232–1241.
[21] E. Sourtiji, S.F. Hosseinizadeh, M. Gorji-Bandpy, J.M. Khodadadi, Computational study of turbulent forced convection flow in a square cavity with ventilation ports, *Numerical Heat Transfer, Part A* 59 (2011) 954–969.
[22] S.C. Saha, Unsteady natural convection in a triangular enclosure under isothermal heating, *Energy and Buildings* 43 (2011) 695–703.
[23] A. Sojoudia, S.C. Saha, Y.T. Gu, Natural convection due to differential heating of inclined walls and heat source placed on bottom wall of an attic shaped space, *Energy and Buildings* 89 (2015) 153–162.
[24] H. Cui, F. Xu, S.C. Saha, A three-dimensional simulation of transient natural convection in a triangular cavity, *International Journal of Heat and Mass Transfer* 85 (2015) 1012-1022.
[25] S.C. Saha, M.M.K. Khan, A review of natural convection and heat transfer in attic-shaped space, *Energy and Buildings* 43 (2011) 2564–2571.
[26] B.E. Launder, D.B. Spalding, The numerical computation of turbulent flows, *Computer Methods in Applied Mechanics and Engineering* 3 (1974) 269–289.
[27] I.V. Miroshnichenko, M.A. Sheremet, Numerical simulation of turbulent natural convection combined with surface thermal radiation in a square cavity, *International Journal of Numerical Methods for Heat & Fluid Flow* 25 (2015) 1600–1618.
[28] I.V. Miroshnichenko, M.A. Sheremet, A.A. Mohamad, Numerical simulation of a conjugate turbulent natural convection combined with surface thermal radiation in an enclosure with a heat source, *International Journal of Thermal Sciences* 109 (2016) 172–181.
[29] M.A. Sheremet, I.V. Miroshnichenko, Numerical study of turbulent natural convection in a cube having finite thickness heat-conducting walls, *Heat Mass Transfer* 51 (2015) 1559–1569.
[30] R. Siegel, J.R. Howell, *Thermal Radiation Heat Transfer*, Taylor & Francis, London, 2002.
[31] A.A. Samarskii, *Theory of difference schemes*, Nauka, Moscow, 1977.
[32] S.G. Martyushev, M.A. Sheremet, Conjugate natural convection combined with surface thermal radiation in an air filled cavity with internal heat source, *International Journal of Thermal Sciences* 76 (2014) 51–67.
[33] F. Ampofo, T.G. Karayiannis, Experimental benchmark data for turbulent natural convection in an air filled square cavity, *International Journal of Heat and Mass Transfer* 46 (2003) 3551–3572.
[34] H. Dixit, V. Babu, Simulation of high Rayleigh number natural convection in a square cavity using the lattice Boltzmann method, *International Journal of Heat and Mass Transfer* 49 (2006) 727–739.
[35] C. Zhuo, C. Zhong, LES-based filter-matrix lattice Boltzmann model for simulating turbulent natural convection in a square cavity, *International Journal of Heat and Fluid Flow* 42 (2013) 10–22.
[36] P. Le Quere, Accurate solutions to the square thermally driven cavity at high Rayleigh number, *Computers & Fluids* 20 (1991) 29–41.
[37] G. Yang, J.Y. Wu, Effects of natural convection, wall thermal conduction, and thermal radiation on heat transfer uniformity at a heated plate located at the bottom of a three-dimensional rectangular enclosure, *Numerical Heat Transfer, Part A: Applications* 69 (2016) 589–606.